

Molecular enhancement of Balmer emissions following foil-induced dissociation of fast H_2^+ and H_3^+ ions

Hisao Kobayashi* and Nobuo Oda

Research Laboratory for Nuclear Reactors, Tokyo Institute of Technology, Ookayama, Meguro-ku, Tokyo 152, Japan

(Received 16 January 1984)

Relative emission yields of Balmer lines as functions of the dwell time ($t_D=0.97\text{--}54.1$ fs) in thin carbon foils ($2\text{--}68\ \mu\text{g}/\text{cm}^2$) have been measured with (0.2–0.8)-MeV/amu H^+ , H_2^+ , and H_3^+ incident on thin carbon foils. Large molecular effects for emission yields of Balmer lines have been observed for H_2^+ and H_3^+ , where the molecular effect for H_3^+ is larger than that for H_2^+ . The molecular effects for H_2^+ and H_3^+ depend on the principal quantum number ($n=3\text{--}6$), but this n dependence disappears at the largest t_D ($=54.1$ fs). The molecular effects rapidly decrease with increasing t_D in the small- t_D (≤ 2 fs) region and more slowly decrease in the large- t_D (≥ 2 fs) region. The magnitudes of the molecular effects at the largest t_D ($=54.1$ fs) are in good agreement with those by Andresen *et al.* [Phys. Scr. 19, 335 (1979)]. Relative populations of n -state hydrogens in the large- t_D (≥ 2 fs) region have been derived from the relative yields of Balmer lines as functions of n and t_D . The molecular enhancement for relative populations of n -state hydrogens for H_2^+ depends on n and t_D , and decreases with increasing t_D and increases with increasing n . Some discussions are presented on the mechanism of production of excited $H(n)$ atoms from incident H^+ and of $H(n)+H^+$ or $2H^+$ breakup fragments from incident H_2^+ (H_3^+).

I. INTRODUCTION

Recently, the molecular effect for yields of neutral hydrogen atoms H^0 emerging from very thin carbon foils bombarded with swift beams ($v \gg v_0 = e^2/\hbar$) of H_2^+ and H_3^+ ions has been studied as a function of the dwell time (time spent in a foil) t_D .¹ The observed molecular effect can be separated into two t_D regions. (a) For $t_D \leq 2$ fs ($\equiv 2 \times 10^{-15}$ s), the overproduction of neutrals is very large but rapidly decreases with increasing t_D . (b) For $t_D \geq 2$ fs, the overproduction of neutrals is also observed but diminishes slowly with t_D , whereas for the production of the neutral fraction for the incident H^0 beam an equilibrium is completely achieved even at $t_D \sim 1.5$ fs.^{1,2}

When incident H_2^+ molecules traverse a thin foil at 0.4–1.2 MeV/amu, the dwell-time dependence of the yield of emergent H_2^+ has also shown the existence of two well-separated transmission regimes,^{3,4} corresponding to the above two t_D regions, i.e., the original regime where the incident species (diproton) carry their original electron(s) and the reconstitution regime where H_2^+ is reconstituted by the process of target electron capture after the loss of the incident electron(s). Concerning the reconstitution of H_2^+ , Cue *et al.*⁴ have estimated the probability for the diproton to capture a target electron as a function of the effective nuclear charge of the molecular orbital (MO) states which depends on the internuclear distance at the exit side of the thin foil.

For incident H_3^+ , recent data^{3,5,6} show that the reconstitution of H_3^+ is not observable, while the yield of emergent H_2^+ exhibits the same trend as that for incident H_2^+ in the t_D region corresponding to the reconstitution regime. No clear explanation for the H_2^+ formation for incident H_3^+ is reported as yet. However, a model similar to the reconstitution model for incident H_2^+ will be possi-

ble to apply to the production of H_2^+ from a breakup triproton system for incident H_3^+ .

Transmission data mentioned above may lead to an idea that the overproduction of neutrals for incident H_2^+ and H_3^+ arises mainly from an enhancement of the electron-capture probability to the dissociative molecular orbitals which subsequently lead to the production of an H^0 atom plus a proton. As the by-product of the reconstitution model, Cue *et al.*⁴ have also calculated the ratio of the yield of H^0 per nucleon for incident H_2^+ to that for incident H^+ in the reconstitution regime. The estimated yield ratio gives the t_D dependence similar to, but of the magnitude markedly smaller than, that measured by Gaillard *et al.*¹ Cue *et al.* took account of only the $1s\sigma_g$ and the $2p\sigma_u$ MO states of H_2^+ , whereas the measured H^0 yield contains all the hydrogen atoms $H(n)$ with $n=1,2,\dots,\infty$, where n is the principal quantum number. Therefore, the discrepancy between calculation and experiment may be attributable to the existence of dissociative MO states which lead to various sets of breakup fragments, $H(n)+H^+$, where much higher molecular effects for the $H(n \geq 2)$ production than for the $H(1s)$ production will be expected to explain the discrepancy. The existence of the dissociative MO states will be closely connected with the observed energy-angular distributions of H^0 atoms.^{7–10} Furthermore, it is expected that the above conjecture should be consistent with the beam-foil experiments^{11–17} which have shown molecular effects for emission yields of Lyman and Balmer photons from the breakup fragments $H(n \geq 2)$ much larger than that for total neutrals as functions of t_D .

The electron-capture probability to the dissociative MO state is very sensitive to the value of the effective nuclear charge and the latter strongly correlates to the internuclear distance(s) (or t_D) and to the n value of the breakup

fragment $H(n)$ dissociated from the corresponding MO state. Therefore, detailed studies of the excited breakup fragments as functions of n and t_D should give data fruitful to elucidate the interactions of the molecular ions with thin foils.

Several studies on the n -state hydrogen atoms excited by thin foils have been reported to date using the beam-foil spectroscopy. Gabrielse¹¹ and Brooks and Berry¹² have measured the Lyman- α emission yields as functions of t_D in carbon foils for H^+ , H_2^+ , and H_3^+ (0.2–1.75 MeV/amu) and observed the molecular effect for the emission yields. Bukow *et al.*¹³ have observed the molecular effects for Lyman- α and Balmer- α emission yields for H^+ , H_2^+ , and H_3^+ (50–200 keV/amu) at relatively large values of t_D (7–14 fs). Similarly, Andresen *et al.*¹⁴ have measured Balmer emission yields for H^+ , H_2^+ , and H_3^+ for larger t_D (27 fs for 100 keV/amu and 55 fs for 50 keV/amu), and shown the n -independent molecular effect for the n -state populations for $n \geq 3$. Astner *et al.*¹⁵ have also reported similar results for 50-keV/amu hydrogen and deuteron molecular ions at $t_D = 6$ –23 fs. We have recently measured Balmer emissions for H^+ , H_2^+ , and H_3^+ incident on 2–37 $\mu\text{g}/\text{cm}^2$ carbon foils at 0.5 and 0.8 MeV/amu,^{16,17} where the range of t_D is from 0.97 to 18.0 fs, and observed the relatively large n -dependent molecular effect for the emission yields.

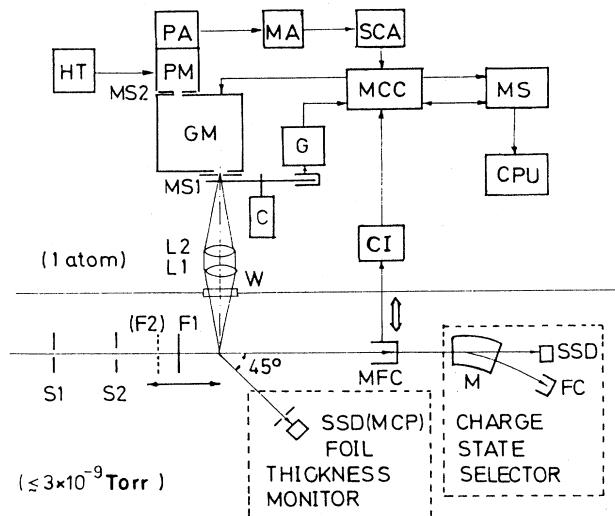
A detailed description of measurements is presented in the present paper, covering wider ranges of t_D as well as of projectile energies. Measured emission yields of Balmer photons are converted to the relative populations of the n states ($n = 3$ –6) in hydrogen fragments, for which the molecular effects are much larger than that for the total neutral H^0 in the reconstitution regime. These molecular effects are discussed in relation to the reconstitution model.

II. EXPERIMENTAL

Hydrogen ions H^+ , H_2^+ , and H_3^+ were accelerated to the energy range between 0.2 and 0.8 MeV/amu by the 3 MV Pelletron accelerator with a duoplasmatron ion source at the Tokyo Institute of Technology. A schematic diagram of the experimental apparatus is shown in Fig. 1.

Three different experimental arrangements have been used to measure (a) the emission yields of Balmer lines of emerging neutral atoms H^0 from a carbon foil for incident molecular ions H_2^+ and H_3^+ ; (b) thicknesses, the uniformity, and the density of the carbon foils; and (c) the neutral fraction in the total transmitted beam for incident atomic ions H^+ and H^0 .

In arrangements (a) and (b), a movable Faraday cup (MFC, Fig. 1) was inserted on the beam line behind a target foil (F1) and was used for the beam current normalization in the optical and the thickness measurements. In arrangement (b), a foil holder wheel was moved along the beam line and the target foil F1 was placed on the point of intersection of the beam line and the 45° detection axis of the foil-thickness monitor. In arrangement (c), the MFC was removed and a charge state selector which consists of a magnetic analyzer (M), a neutral hydrogen beam detector [solid state detector (SSD)], and a proton beam



NOT TO SCALE

FIG. 1. Schematic diagram of the experimental setup for the beam-foil experiment and the photon counting system. S1 and S2, 0.5 and 2.0 mm inner diameter apertures, respectively, which are separated by 1194 mm; F1, target foil; F2, dissociation foil; MFC, movable Faraday cup; M, magnetic analyzer; SSD, solid-state detector; FC, Faraday cup; W, quartz window; L1 and L2, quartz lenses having a 30-cm focal length; C, 70-Hz chopper; G, chopper gate signal generator; GM, grating monochromator having an entrance slit MS1 and an exit slit MS2; HT, high voltage supply; PM, photomultiplier; PA, preamplifier; MA, main amplifier; SCA, single channel analyzer; MCC, monochromator and multichannel scaler control circuit; MS, multichannel scaler; CI, current integrator; and CPU, microprocessor.

detector [Faraday cup (FC)] was used to measure the neutral fraction.

After being energy and mass analyzed and before entering a scattering chamber, the incident beams were passed through two apertures 1194 mm apart (S1 and S2) whose diameters were selected to be 0.5 and 2.0 mm, respectively. The beams were collimated to less than 2.3 mm in diameter at the target-foil position, and the angular spread of the beams was less than 2.1 mrad.

The collimator system and the cylindrical collision chamber, which has an inner diameter of 30 cm, were pumped with a combination of four ion pumps, two titanium getter pumps, and two liquid-nitrogen traps. The vacuum in the collision chamber was typically kept to better than 3×10^{-9} Torr even during measurements.

Beams were passed through the target foils F1 mounted on the movable and rotatable foil holder wheel which has an opening window and can hold 15 foils with different thicknesses. One or two windows of the holder wheel were equipped with double-foil systems which consist of the target foil F1 and a second foil (F2, 20 $\mu\text{g}/\text{cm}^2$). The second foil F2 was set 13 mm upstream from the target foil F1, and served as a stripper which produces a charge-equilibrated H^+ beam from the H_2^+ and H_3^+ beams, keeping the other experimental conditions the

same. Mean internuclear distances of the dissociated fragments produced by the double-foil system (F1 + F2) are so large at the foil F1 that dissociated fragments may be regarded to behave independently to each other.

For the usual type of beam-foil experiments, the beams were finally collected by MFC which was located 160 mm downstream from F1. The entrance aperture of MFC was 25 mm in diameter and was large enough to collect all the secondary fragment ions passing through the thickest foil used as well as primary ions.

The Balmer radiation emitted 5 mm downstream from F1 was focused on an entrance slit (MS1) of a modified Cerny-Turner-type scanning grating monochromator (GM) equipped with a Hamamatsu R649S photomultiplier (PM) by a 6-cm-diam quartz lens system (L1 and L2) with a focal length of 30 cm.

The monochromator GM with a focal length of 30 cm and f value of 5.2 is equipped with a 52×52 mm square grating having grooves of 1200 lines/mm which gives reciprocal dispersion of $25 \text{ \AA}/\text{mm}$. The sizes of the entrance and exit slits (MS1 and MS2) are variable from 0 to 12 mm in height (vertical to the beam) and from 0 to 5 mm in width (parallel to the beam). Since the emitted Balmer intensities were extremely weak at the beam energy of 0.8 MeV/amu which was the highest energy in the present measurements, we could not reduce the slit width to below 3 mm for the slit height of 12 mm used through measurements. This leads to a poor resolution of 89 \AA full width at half maximum (FWHM).

The optical axis was set at a right angle to the beam direction. The lens system has a conical solid angle of 0.025 sr and the Doppler broadening is estimated to be $12 \pm 1 \text{ \AA}$ FWHM by the measurement of the H_α (6563 \AA) line for 0.5-MeV/amu ($v/c=0.04$) H_3^+ passing through a $10\text{-}\mu\text{g}/\text{cm}^2$ carbon foil.

The alignment of the optical system [W, L1, L2, MS1, GM, and MS2 (where W is the quartz window)] was attained using a He-Ne laser ($\lambda=6328 \text{ \AA}$). To improve the signal-to-noise ratio, a chopper (C) was placed between L2 and MS1 in the optical path. The chopper gate signals were generated by a circuit G with the duty rate being 38.1% at 70 Hz.

The photon intensities of Balmer lines were determined from the peak area of each line. The spectra of Balmer lines for $n \geq 6$ (H_δ , H_ϵ , etc.) are superposed on each other because of the large FWHM. The peak area was estimated by a deconvolution technique from the measured spectral shape which could be approximated by an isosceles triangle. The typical photon counting rate was $130 H_\alpha$ counts per μC at 0.5 MeV/amu of H_2^+ .

A block diagram of electronics used is shown in Fig. 1. Balmer photons chopped by G with 70 Hz were detected by PM. The output pulses of PM were amplified and discriminated by conventional electronics, which are composed of a preamplifier (PA), a main amplifier (MA), and a single-channel analyzer (SCA), and were fed into a monochromator and multichannel scaler control circuit (MCC) constructed in our laboratory. The programmable MCC is a central part of our photon spectrometer system. Roles played by MCC are, first, gating of the chopped photon signals using reference signals from the chopper

gate generator G and, second, repetitive scanning of a multichannel scaler (MS) and GM whose scanning speed is controlled by a preset beam charge measured with MFC followed by a current integrator (CI). Background (stray light and PM thermal noise) subtractions, peak-area calculations, statistical treatments, and data corrections were performed by a microprocessor central processing unit (CPU). In summary, the functions of the photon counting system are as follows: (i) A selected range of wavelength is automatically and repetitively scanned, (ii) the scanning speed is controlled by a preset beam charge, and (iii) one-to-one correspondence between the channel number of MS and the wavelength is established.

The thicknesses of carbon foils were measured with a quartz thickness monitor at the manufacturing stage of foils by evaporation and later by the optical-interference method. All foils were inspected for pinholes and folds by a microscope. After foils were attached on the foil holder wheel, the foil thicknesses were further measured with a foil-thickness monitor utilizing the Rutherford scatterings during measurements in order to observe the uniformity of foils, the foil-thickening effect by ion bombardments, and also the foil thicknesses in units of $\mu\text{g}/\text{cm}^2$. From these measurements, the density of carbon foils was determined to be $1.66 \pm 0.10 \text{ g}/\text{cm}^3$, which is in good agreement with the value of Gaillard *et al.*¹ Accuracies of foil thicknesses were found, for a beam size of 1 mm in diameter, to be ± 0.1 – $\pm 0.5 \mu\text{g}/\text{cm}^2$ for the thickness range between 2 and $10 \mu\text{g}/\text{cm}^2$ and to be ± 0.3 – $\pm 2.7 \mu\text{g}/\text{cm}^2$ for foils thicker than $10 \mu\text{g}/\text{cm}^2$, including the uniformity fluctuation. A typical change of the Balmer line intensity due to foil thickening was 0.32% per mC of beam current for the $2 \mu\text{g}/\text{cm}^2$ foil, in which case foil thickening per mC was $0.1 \mu\text{g}/\text{cm}^2$.

The absolute projectile energy can be determined with an uncertainty of $\pm 5 \text{ keV}$, but its precision was estimated to be less than $\pm 1 \text{ keV}$, typically $\pm 200 \text{ eV}$. Energy losses in carbon foils were estimated using data by Andersen and Ziegler¹⁸ and primary energies were adjusted for the emergent velocities after foils to be the same for various foil thicknesses.

In order to obtain initial population probabilities, one must determine the intensities of the Balmer lines immediately after the foils, before the cascading rearrangements take place. The Balmer line intensities were measured at 5 mm downstream from the target F1 and the intensities at the origin were obtained using decay curves which were previously measured. For example, the decay of Balmer- α emission yield at 5 mm was 3% for 0.5-MeV/amu H_2^+ and H_3^+ . The cascading rearrangements were estimated as shown in Appendix A.

The measured beam currents were corrected for the neutral fractions and, typically, the maximum correction was estimated to be 1.2% to the measured emission yield ratio for H_2^+ . The measured photon counts were corrected for the wavelength response of the whole optical system, including the transmission efficiency of the L1, L2, and GM and the quantum efficiency of the PM, using a calibrated tungsten halogen lamp (Osram model 64425, 12 V, 20 W, 2850 K). Further, the light intensities were corrected for the difference in the time intervals of light

observation seen by the optical system due to the difference in the projectile energies, 0.2–0.8 MeV/amu.

III. DATA ANALYSIS

A. Balmer emission yield ratios

Molecular enhancement $R_Y(n, t_D)$ as a function of the principal quantum number n and the dwell time t_D is written as

$$R_Y(n, t_D) = Y^{\text{mol}}(n, t_D) / Y^{\text{H}^+}(n, \infty), \quad (1)$$

where $Y^{\text{mol}}(n, t_D)$ is the relative Balmer emission yield per proton for incident molecular ions H_2^+ and H_3^+ , and $Y^{\text{H}^+}(n, \infty)$ is the yield for the proton beam under the equilibrium charge condition. The yield $Y^{\text{H}^+}(n, \infty)$ can be measured using the double foil for incident molecular ions. The double foil is used to dissociate the molecular ions and produce the equilibrated fragment beams which are mostly composed of protons in the energy range in the present measurements and the contribution of minor fragment components such as H^0 was corrected for the derivation of the $Y^{\text{H}^+}(n, \infty)$. The use of the double foil ensures that fragments are well separated via the Coulomb repulsion mechanism at the position of foil F1. For example, Kanter *et al.*⁹ measured the joint energy-angular distribution for proton arising from the dissociation of 1.4-MeV H_2^+ in an 88-Å-thick carbon foil, which gives the internuclear distance of $\sim 70 \mu\text{m}$ at 13 mm downstream from the foil. The same order of internuclear distances are expected under our experimental conditions, which are long enough to assure that there is no correlation effect between fragments. Hereafter, the yield measured by the double foil experiment is denoted as $Y^{\text{H}^+}(n, \infty)$.

B. Population ratios of n -excited states

The relative population of the n -excited state at t_D , $P(n, t_D)$, can be given by

$$P(n, t_D) = \sum_{l=0}^{n-1} P(nl, t_D), \quad (2)$$

where $P(nl, t_D)$ are the relative population of the substate (nl) of emergent hydrogen atoms at t_D . The relative Balmer emission yield $Y(n, t_D)$ ($n \geq 3$) is connected to the substate populations by the following relation:

$$Y(n, t_D) = \xi \sum_{l=0}^2 \sum_{l'=0}^1 A_{nl2l'} P(nl, t_D), \quad (3)$$

where $A_{nl2l'}$ is the transition probability for the transition from the substate (nl) to the substate ($2l'$), and ξ is the geometrical detection efficiency of the optical system. The values of $A_{nl2l'}$ are given by Wiese *et al.*¹⁹ The efficiency depends only on the projectile velocity, if other experimental conditions, such as the slit width of GM, the amplifier gain, the discriminator threshold, etc., are kept the same. The contribution of the cascade process to the Balmer emission is estimated to be negligibly small (see Appendix A) and is disregarded in Eq. (3).

When the average transition probability $\langle A_n(t_D) \rangle$ is defined as a function of t_D by the relation

$$\langle A_n(t_D) \rangle = \frac{\left[\sum_{l=0}^2 \sum_{l'=0}^1 A_{nl2l'} P(nl, t_D) \right]}{\left[\sum_{l=0}^{n-1} P(nl, t_D) \right]}, \quad (4)$$

we have from Eqs. (2) and (3)

$$P(n, t_D) = (1/\xi) Y(n, t_D) / \langle A_n(t_D) \rangle. \quad (5)$$

If the value of $\langle A_n(t_D) \rangle$ defined by Eq. (4) is known, the relative population of the n state can be derived from Eq. (5) using the relative Balmer emission yield $Y(n, t_D)$.

The ratio of the n -state relative population per proton for the molecular ion, $P^{\text{mol}}(n, t_D)$, to that for H^+ , $P^{\text{H}^+}(n, \infty)$, is defined as

$$R_P(n, t_D) = P^{\text{mol}}(n, t_D) / P^{\text{H}^+}(n, \infty), \quad (6)$$

where $P^{\text{H}^+}(n, \infty)$ is the corresponding population obtained by the double-foil measurement. If $Y(n, t_D)$ and $\langle A_n(t_D) \rangle$ are known for proton and molecular ions, Eq. (6) is rewritten using Eq. (5) as follows:

$$R_P(n, t_D) = [Y^{\text{mol}}(n, t_D) / Y^{\text{H}^+}(n, \infty)] \times [\langle A_n^{\text{H}^+}(t_D) \rangle / \langle A_n^{\text{mol}}(t_D) \rangle]. \quad (7)$$

Now, the ratio $R_P(n, t_D)$ becomes essentially independent of the geometrical efficiency ξ as well as the wavelength response of the optical system.

In order to obtain $\langle A_n(t_D) \rangle$ from Eq. (4), the relative initial populations $P(nl, t_D)$ of the nl substates must be known for both proton and molecular ions and for various dwell times. Unfortunately, the measurements of $P(nl, t_D)$ have, so far, only been done for $n=2$ and 3 and are limited with respect to ion species, ion velocities, and dwell times.^{13,20,21}

Bukow *et al.*¹³ experimentally derived the ratio of initial populations, $P(3p)/P(3s)$ and $P(3d)/P(3s)$, for proton and molecular ions with the energy range from 50 to 200 keV/amu incident on a carbon foil ($7 \pm 2 \mu\text{g}/\text{cm}^2$), corresponding to the dwell times from 7 to 12 fs. They assumed that ratios for H_2^+ and H_3^+ are of the same value and are independent of the t_D value. Their ratios $P(3p)/P(3s)$ and $P(3d)/P(3s)$ are 0.608 and 0.422 for H^+ , and 1.08 and 1.29 for H_2^+ (H_3^+), respectively, and these experimental values are smaller than those derived on the statistical model.

Alguard and Drake²⁰ obtained the ratio of substate excitation cross sections from the beam-foil measurement of the Stark beat of Lyman α ($n=2$) and β ($n=3$) for incident protons. Their experimental data for H^+ show that the cross-section ratios σ_{2s}/σ_{2p} , σ_{3s}/σ_{3p} , and σ_{3d}/σ_{3p} may be regarded to be independent of the projectile energy between 255 and 508 keV within experimental errors, supporting the results of Bukow *et al.*¹³ Taking into consideration the above experimental results,^{13,20} the following assumptions are introduced to analyze our experimental results.

Assumption 1. (a) Regardless of n , the ratios $P(np)/P(ns)$ and $P(nd)/P(ns)$ are independent of projec-

tile energy at least up to 800 keV/amu for protons and molecular ions. (b) The ratios are also independent of t_D for molecular ions. (c) Each ratio has the same value for H_2^+ and H_3^+ .

Although assumption 1(c) is based on the assumption by Bukow *et al.*, since their data analysis for the H_3^+ data seems to be questionable, more detailed studies would be needed with respect to initial substate populations for H_3^+ and, therefore, the populations for H_3^+ are derived only for reference in the following.

The ratios for molecular ions should finally approach that for protons with increasing t_D . This apparently contradicts the assertion of assumption 1(b). Therefore, the application of assumption 1(b) must be limited to some t_D range which is not so much extended over the range in the measurement of Bukow *et al.* The n -state molecular enhancement in the t_D (≥ 2 fs) region may be interpreted as an enhancement of the cross section for electron capture to the corresponding molecular orbital at the internuclear distance d . Then, the electron-capture cross section depends on d in the vicinity of the exit surface of the foil. In the LCAO approximation, the electron-capture cross section depends on the overlap integral of the wave functions of excited hydrogen atoms as a function of d . Therefore, the diameter or radius of the excited hydrogen atom is a good parameter to describe the molecular enhancement. Later, it will be shown experimentally that the molecular enhancement does not disappear even when d exceeds the corresponding orbital diameter but slowly decreases with increasing d . From the above discussion assumption 1(b) should be modified as follows.

Assumption 1(b'). The ratios for molecular ions are independent of t_D only in the t_D range between 2 fs and the t_D value corresponding to the d value equal to the orbital diameter of the n -excited hydrogen atom.

We can write $P(nl, t_D)$ as $P(nl)$ for $n=2$ and 3 on this assumption in the following.

No data on $P(nl, t_D)$ have been reported for $n \geq 4$. Therefore, additional assumptions are required with respect to $\langle A_n(t_D) \rangle$.

Assumption 2(a). For $l \leq 2$, the ratios $P(nl)/P(ns)$ are equal to $P(3l)/P(3s)$ for all n values of $n \geq 4$.

Hopkins and Brentano²² theoretically investigated the high n -state populations in hydrogenlike ions immediately after emerging from a solid foil and derived the general form for the populations

$$P(nl) = P(1,1)n^{-b}(l/n)^h, \quad n \geq 4, l \geq 1 \quad (8)$$

where $P(1,1)$, b , and h are parameters to be experimentally determined. Then we introduce the following assumption.

Assumption 2(b). The values of $P(nl)/P(ns)$ for $n \geq 4$ and $l \geq 3$ are estimated by extrapolation of $P(3l)/P(3s)$ ($l \leq 2$) to higher l values ($l \geq 3$) using Eq. (8).

IV. RESULTS AND DISCUSSIONS

A. Balmer emission yields and the molecular effect

Relative Balmer emission yields per proton, Y^{H^+} [$\equiv Y^{H^+}(n, \infty)$], $Y^{H_2^+}$ [$\equiv Y^{H_2^+}(n, t_D)$], and $Y^{H_3^+}$ [$\equiv Y^{H_3^+}(n, t_D)$], are plotted against n for $t_D = 0.97$ fs ($2 \mu\text{g}/\text{cm}^2$, 0.8 MeV/amu) and 6.17 fs ($10 \mu\text{g}/\text{cm}^2$, 0.5 MeV/amu) in Fig. 2, where regression lines, assuming a functional form n^{-p} , are also shown. The yield Y^{H^+} is equivalent to that for the equilibrium foil thickness and was measured by the double-foil technique. Error bars in Fig. 2 stand only for statistical errors. In Table I some p values obtained by the regression analysis for 0.97–54.1 fs are shown. For protons, an average p value and its standard deviation are shown as obtained from 18 double-foil measurements for the energy range from 0.2 to 0.8 MeV/amu in Table I. For H_2^+ and H_3^+ , uncertainties indicate the 68% confidence intervals²³ which correspond to the width of one standard deviation.

The following results were obtained. (i) Relative yields $Y^{H_2^+}$ and $Y^{H_3^+}$ are higher than Y^{H^+} for $n=3-6$. (ii) The yield $Y^{H_3^+}$ is higher than $Y^{H_2^+}$. (iii) Yields Y^{H^+} , $Y^{H_2^+}$, and $Y^{H_3^+}$ are all well fitted by a functional form n^{-p} for $n=3-6$, where the values of the exponent p for H_2^+ and H_3^+ are higher than for H^+ . (iv) The value of p for H^+ is independent of proton energies between 0.2 and

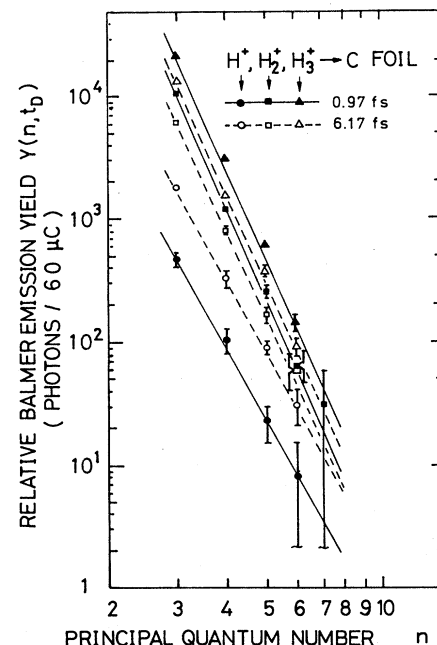


FIG. 2. Relative Balmer emission yields $Y(n, t_D)$ per nucleon per unit beam current ($60 \mu\text{C}$) as functions of the principal quantum number n . Solid symbols and solid lines represent experimental data and least-squares fits to the data, respectively, for 0.8-MeV/amu H^+ , H_2^+ , and H_3^+ at a dwell time of 0.97 fs. Open symbols and dashed lines are those for 0.5 MeV/amu at 6.17 fs. \bullet, \circ, H^+ ; $\blacksquare, \square, H_2^+$; and $\blacktriangle, \triangle, H_3^+$. Error bars represent statistical uncertainties.

TABLE I. Values of p . Emission yields of Balmer photons are fitted by a functional form n^{-p} ($n=3-6$). The values of adjustable parameter p are given for $t_D=0.97-54.1$ fs and for H^+ , H_2^+ , and H_3^+ .

Dwell time (fs)	Projectile energy (MeV/amu)	p values		
		H^+	H_2^+	H_3^+
0.97	0.8		7.03 ± 0.30^a	6.99 ± 0.29^a
1.23	0.5		6.86 ± 0.17	6.81 ± 0.17
6.17	0.5		6.78 ± 0.30	6.97 ± 0.51
22.8	0.5		6.71 ± 0.49	6.70 ± 0.30
29.5	0.3		6.40 ± 0.14	6.79 ± 0.18
54.1	0.3		6.05 ± 0.17	6.48 ± 0.05
∞	0.2-0.8	6.07 ± 0.11^b		

^a68% confidence intervals.

^bThe value for H^+ is that corresponding to the foil with infinite thickness and the listed mean value and the standard deviation are for the 18 double-foil measurements for proton energies between 0.2 and 0.8 MeV.

0.8 MeV within experimental uncertainties, and the average value of p is 6.07 ± 0.11 ($n=3-6$) for 18 double-foil measurements with different combinations of energies and species of incident projectiles, H_2^+ and H_3^+ . Results (i)-(iii) are valid for the whole measured range of the dwell time from 0.97 to 54.1 fs.

Andresen *et al.*¹⁴ and Astner *et al.*¹⁵ estimated the n -state population following the $n^{-4.0}$ scaling law at 25 keV/amu and the $n^{-3.7}$ scaling at 50 keV/amu and 100 keV/amu for H^+ , H_2^+ , H_3^+ , D^+ , D_2^+ , and D_3^+ , assuming an n^{-3} dependence of the transition probability. The exponent in the above scaling law approaches -3 at large velocities. Their p values in the expressions for Balmer emission yields should approach 6 with the increase of energy. Their results are in agreement with some of our results, i.e., $p=6.07 \pm 0.11$ for (0.2-0.8)-MeV H^+ and $p=6.05 \pm 0.08$ for 0.3-MeV/amu H_2^+ , at the largest t_D (=54.1 fs), whereas larger p values were observed for other t_D and velocities of H_2^+ and H_3^+ .

The ratios $R_Y(n, t_D)$ are shown as functions of n at $t_D=0.97, 1.2, 22.8,$ and 54.1 fs for H_2^+ and H_3^+ in Fig. 3, where regression lines assuming a functional form n^{-q} are also shown. The values of q so obtained agree well with the p values for molecular ions subtracted by that for H^+ within experimental uncertainties. The values of q slowly decrease with the increase of t_D for both H_2^+ and H_3^+ and should eventually approach zero at some large dwell time. At the largest t_D (=54.1 fs) used, the value q for 0.3-MeV/amu H_2^+ and H_3^+ is close to zero and found to be -0.05 ± 0.08 and $+0.37 \pm 0.27$, respectively; in good agreement with that of Andresen *et al.*¹⁴ within experimental uncertainties.

The ratios $R_Y(n, t_D)$ for $n=3$ (H_α) and $n=4$ (H_β) are shown as functions of t_D for 0.3, 0.4, 0.5, and 0.8 MeV/amu in Figs. 4(a) and 4(b), respectively. The ratios for the yields of total neutrals ($n \geq 1$), $\Phi_0^{\text{mol}}/\Phi_0^{\text{atom}}$,¹ are also shown by a thin solid curve for H_3^+ and a thin dashed curve for H_2^+ in Fig. 4. The values of d for H_2^+ and H_3^+ calculated on a simple Coulomb repulsion model are for convenience shown on the upper part of Fig. 4(a).

The ratios $R_Y(n, t_D)$ ($n \geq 3$) for H_2^+ and H_3^+ decrease very rapidly in the t_D (≤ 2 fs) region and decrease slowly in the t_D (≥ 2 fs) region with the increasing t_D . In this figure, a similar tendency is seen between $R_Y(n, t_D)$ for $n \geq 3$ and $\Phi_0^{\text{mol}}/\Phi_0^{\text{atom}}$,¹ and also $R_Y(2, t_D)$ measured by Brooks and Berry¹² (not shown in Fig. 4), but the magnitudes of $R_Y(n, t_D)$ ($n \geq 3$) are much greater than those of $\Phi_0^{\text{mol}}/\Phi_0^{\text{atom}}$ and $R_Y(2, t_D)$. While $\Phi_0^{\text{mol}}/\Phi_0^{\text{atom}}$ approaches unity as t_D increases to ~ 15 fs, $R_Y(n, t_D)$ for $n \geq 3$ still shows appreciable molecular enhancement even at the

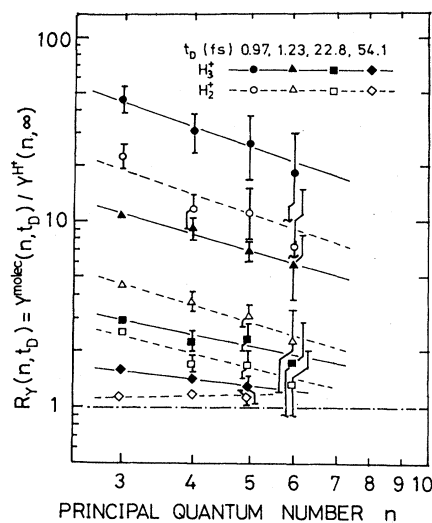


FIG. 3. Molecular effects for Balmer emission yields, $R_Y(n, t_D) = Y^{\text{mol}}(n, t_D) / Y^{\text{H}^+}(n, \infty)$, as functions of n . Symbols and lines represent experimental data and least-squares fits to the data, respectively. Solid symbols and solid lines are for H_3^+ , and open symbols and dashed lines for H_2^+ . \bullet, \circ , 0.8 MeV/amu and 0.97 fs; $\blacktriangle, \triangle$, 0.5 MeV/amu and 1.23 fs; \blacksquare, \square , 0.5 MeV/amu and 22.8 fs; and \blacklozenge, \diamond , 0.3 MeV/amu and 54.1 fs. Error bars represent statistical uncertainties.

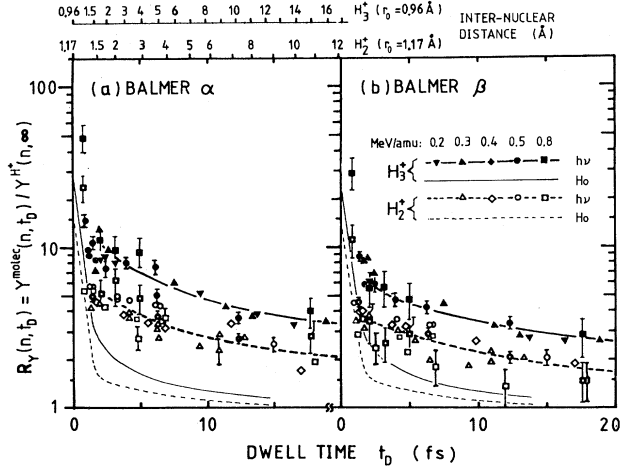


FIG. 4. (a) Molecular effects for Balmer emission yields, $R_Y(n, t_D) = Y^{\text{mol}}(n, t_D) / Y^{\text{H}^+}(n, \infty)$, as functions of the dwell time t_D for H_3^+ (solid symbols and solid curve) and H_2^+ (open symbols and dashed curve) for $n=3$ (Balmer α) and (b) for $n=4$ (Balmer β). $\blacksquare, \square, 0.8$ MeV/amu; $\bullet, \circ, 0.5$ MeV/amu; $\blacklozenge, \diamond, 0.4$ MeV/amu; $\blacktriangle, \triangle, 0.3$ MeV/amu; and $\blacktriangledown, \triangledown, 0.2$ MeV/amu. Error bars statistical uncertainties. Production ratios for total neutral hydrogens, $\Phi_0^{\text{mol}} / \Phi_0^{\text{atom}}$, given by Gaillard *et al.* (Ref. 1) are also shown for H_3^+ (thin solid curve) and H_2^+ (thin dashed curve). Internuclear distances in \AA are shown for H_3^+ (initial distance $d_0=0.96$ \AA) and for H_2^+ ($d_0=1.17$ \AA) at the upper part of (a).

largest t_D . The ratios $R_Y(n, 54.1$ fs) for $n=3, 4$, and 5 are 1.13 ± 0.02 , 1.15 ± 0.05 , and 1.16 ± 0.12 for 0.3 -MeV/amu H_2^+ ; and 1.59 ± 0.04 , 1.42 ± 0.06 , and 1.32 ± 0.16 for 0.3 -MeV/amu H_3^+ , respectively. These ratios were close to those for the low-energy studies (25 and 100 keV/amu; $t_D=55$ and 27 fs) by Andersen *et al.*¹⁴ which are 1.20 for H_2^+ and 1.45 for H_3^+ .

B. Molecular effect for n -state populations

1. n dependence of beam-foil excited populations

In order to derive the average transition probabilities from n (≥ 3) states to the $n=2$ state, $\langle A_n(t_D) \rangle$, with the use of Eq. (4), values of transition probability A_{n2l}

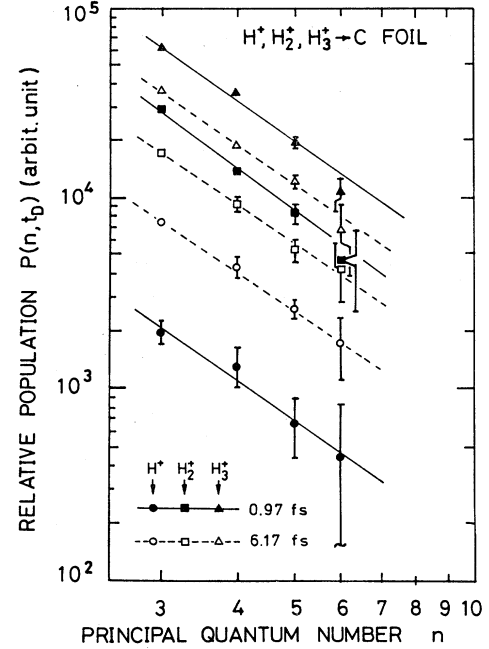


FIG. 5. Relative n -state populations $P(n, t_D)$ as functions of n for 0.8 -MeV/amu H^+ , H_2^+ , and H_3^+ at $t_D=0.97$ fs and those for 0.5 MeV/amu at 6.17 fs. Values $P(n, t_D)$ are derived from data in Fig. 2, using Eq. (5). Notations are the same as in Fig. 2.

($n \geq 3$) and of the substate population ratios $P(nl)/P(ns)$ ($n \geq 3$) are needed. Values of A_{n2l} ($n \geq 3$) were given by Wiese *et al.*¹⁹ and values of $P(nl)/P(ns)$ ($n \geq 3$) are derived with the use of assumptions 1 and 2, combined with the empirical values for $P(3l)/P(3s)$ by Bukow *et al.*¹³ Now, the relative n -state populations $P(n, t_D)$ can be estimated from measured Y values (Y^{H^+} , $Y^{\text{H}_2^+}$, and $Y^{\text{H}_3^+}$) as functions of n and t_D by Eq. (5). Two sets of $P(n, t_D)$ are plotted as functions of n at $t_D=0.97$ fs for 0.8 -MeV/amu H^+ , H_2^+ , and H_3^+ , and at 6.2 fs for 0.5 MeV/amu in Fig. 5. Straight and dashed lines in Fig. 5 are regression lines obtained assuming a functional form n^{-z} for $P(n, t_D)$ at 0.97 and 6.2 fs, respectively, where z is an adjustable parameter.

TABLE II. Values of z . The relative n -state populations $P(n, t_D)$ are fitted by a functional form n^{-z} ($n=3-6$). The values of adjustable parameter z are given for $t_D=0.97-54.1$ fs and for H^+ , H_2^+ , and H_3^+ . The t_D values correspond to those given in Table I.

Dwell time (fs)	Projectile energy (MeV/amu)	z values		
		H^+	H_2^+	H_3^+
0.97	0.8		2.33 ± 0.30^a	2.21 ± 0.16^a
1.23	0.5		2.23 ± 0.29	2.18 ± 0.30
6.17	0.5		2.09 ± 0.13	2.19 ± 0.13
22.8	0.5		1.92 ± 0.34	2.00 ± 0.34
29.5	0.3		1.62 ± 0.02	2.10 ± 0.13
∞	0.2-0.8	2.30 ± 0.11^b		

^a68% confidence intervals.

^bAs in Table I.

Values of z and of the 68% confidence intervals are given for five different t_D values from 0.97 to 29.5 fs in Table II. It is shown in Table II that the z value for H^+ is independent of t_D , for H_2^+ z slowly decreases with t_D in the $t_D (\geq 2$ fs) region, and for H_3^+ z is almost independent of t_D , having slightly lower values than that for H^+ . In Table II, the same t_D values as in Table I are chosen except for 54.1 fs, for the reason that the population ratio for $n=3$ at 54.1 fs, $R_P(3, 54.1$ fs), gives an unreasonably lower value than unity for H_2^+ , while an appreciable molecular effect (enhancement) for emission yield [$R_Y(n, t_D) > 1$] has been observed at 54.1 fs as shown in Fig. 3. This result may be due to the use of the incorrect substate population ratios instead of more correct ratios which are expected to asymptotically approach those for H^+ with increasing t_D . The dwell time 54.1 fs corresponds to $d=35$ Å which is about 2.5 times greater than the average diameter of the hydrogen 3s-state orbit. Therefore, the electron capture to proton process should be independent of the presence of another fragment (proton), that is, the enhancement of the probability for electron capture by the presence of a nearby fragment becomes weaker with increasing d to a magnitude much greater than the diameter of the orbit of interest. The restriction for the t_D range by assumption 1(b') is based on this fact.

2. Population ratios of $n=3$ state

Population ratios $R_P(3, t_D)$ can be derived using Eq. (7) together with assumption 1 and are plotted for (0.2–0.8)-MeV/amu H_3^+ and (0.3–0.8)-MeV/amu H_2^+ as functions of t_D for the $t_D (\geq 2$ fs) region in Fig. 6. In this figure, ratios for the $t_D (\leq 2$ fs) region are not shown. As shown in Appendix B, we can estimate $R_P(3, t_D)$ values from the 3d-3p emission yields which have been obtained by Bukow *et al.* (a_{3d}^0 in Ref. 13) at various t_D , and the results are also shown in Fig. 6 by double circles for H_2^+ , which are in fair agreement with our results within experimental uncertainties. Since the agreement is rather poor for H_3^+ , their values are not shown in Fig. 6. This disagreement for H_3^+ may mean that the relative substate populations in Eq. (4) given by Bukow *et al.* would be valid for H_2^+ but invalid for H_3^+ . Therefore, $P(n, t_D)$ in Fig. 5 and $R_P(n, t_D)$ in Fig. 6 for H_3^+ are shown only as references as already noted in Sec. III.

Many fitting equations have been examined to fit our results, taking into consideration that $R_P(n, t_D)$ as a function of t_D should have the asymptotic value of unity at $t_D = \infty$. The best fitting equation for the regression analysis for the $t_D (\geq 2$ fs) region was found to be

$$R_P(n, t_D) = ke^{-mt_D} + 1, \quad t_D \geq 2 \text{ fs} \quad (9)$$

where k and m are fitting parameters which should generally depend on n . Solid and dashed curves shown in Fig. 6 are the resulting regression curves given by Eq. (9) valid in the $t_D (\geq 2$ fs) region for H_3^+ and H_2^+ , respectively.

The values of d for the initial internuclear distances are 1.17 and 0.96 Å for H_2^+ (Ref. 9) and H_3^+ ,²⁴ respectively, as shown on the upper part of Fig. 6. Average diameters

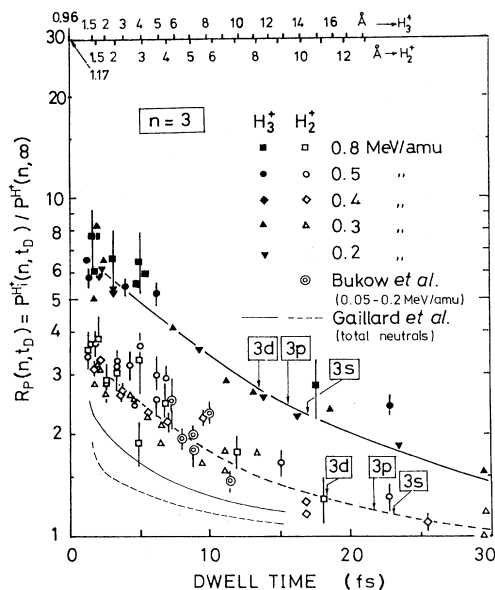


FIG. 6. Molecular effects $R_P(n, t_D)$ for ($n=3$)-state populations as functions of dwell time t_D . Symbols are the same as in Fig. 4 except for double circles which are the values derived from data of Bukow *et al.* (Ref. 13) using Eq. (7). Solid and dashed curves at the $t_D (\geq 2$ fs) region are least-squares fits to data for H_3^+ and H_2^+ , respectively, which are given by Eq. (9). Thin solid and thin dashed curves represent the molecular enhancement for the total neutrals measured by Gaillard *et al.* (Ref. 1) for H_3^+ and H_2^+ , respectively. Arrows represent the average diameters of 3s, 3p, and 3d atomic hydrogen orbits (Ref. 25). Internuclear distances in Å units are shown for H_2^+ and H_3^+ in the upper part of this figure.

of 3s, 3p, and 3d orbits of hydrogen atom are calculated using $2(\frac{1}{2})[3n^2 - l(l+1)]$ (Ref. 25) and are shown by arrows in Fig. 6 for reference.

Thin solid and thin dashed curves in Fig. 6 represent the ratios of the total neutrals ($n \geq 1$) measured by Gaillard *et al.*¹ for H_2^+ and H_3^+ , respectively.

3. Population ratios of $n \geq 4$ states

For $n=3$, to estimate the population ratio $R_P(n, t_D)$ for H_2^+ from Eq. (7) only assumption 1 is needed. However, additional assumptions, 2(a) and 2(b), are required to obtain $R_P(n, t_D)$ for $n \geq 4$. Similar to the case for $n=3$, the values $R_P(n, t_D)$ for $n=4$ and 5 are fitted very well by Eq. (9), and regression curves given by Eq. (9) are shown as semilogarithmic plots of the relation $R_P - 1$ [$R_P \equiv R_P(n, t_D)$] versus t_D for $n=3-5$ in Fig. 7. Hereafter, $R_P - 1$ is called "molecular enhancement." Figure 7 also shows $R_P - 1$ for $n=2$ (squares and solid line) which are derived in the next paragraph, and $\Phi_0^{\text{mol}}/\Phi_0^{\text{atom}} - 1$ (dashed line) given by Gaillard *et al.*¹ It can be seen that the decrease of $R_P - 1$ with increasing t_D becomes slower as the n value increases. In other words, the molecular effects are enhanced to a greater degree with increasing n at

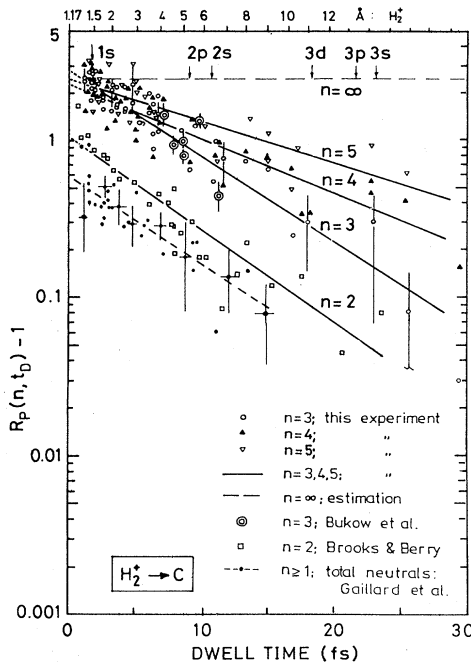


FIG. 7. Molecular enhancements for n -state populations, $R_p(n, t_D) - 1$, as functions of t_D for (0.3–0.8)-MeV/amu H_2^+ . Open circles are for the ($n=3$)-state population and double circles are those derived from data by Bukow *et al.* (Ref. 13). Symbols \blacktriangle and ∇ are for $n=4$ and $n=5$, respectively. Regression lines are shown for $n=3, 4$, and 5 . Long dashed line labeled $n=\infty$ represents our estimation extrapolated to $n=\infty$ (see text). Open squares and their regression line are derived from data of Brooks and Berry for $n=2$ (Ref. 12). Small dots and their regression line (dashed line) are for total neutrals derived from data by Gaillard *et al.* (Ref. 1). Arrows represent the average diameters of several atomic hydrogen orbits. Internuclear distance in \AA is shown for H_2^+ ($d_0=1.17 \text{ \AA}$) in the upper part of this figure.

a fixed t_D in the $t_D (\geq 2 \text{ fs})$ region. This noticeable result will be discussed again in Sec. IV B 6.

4. Population ratios of $n=2$ state

Brooks and Berry¹² measured the molecular effect for yields of Lyman- α emissions following beam-foil excitation of (0.2–1.75)-MeV/amu H_2^+ and H_3^+ . Bickel²¹ estimated initial population ratios $P(2s)/P(2p)$ ($\equiv N_{2s}^0/N_{2p}^0$, in Ref. 21) to be 1.45 and 1.08 for 0.233-MeV/amu H^+ and H_3^+ , respectively, through measurements of Stark-modified mean life of $2s$ and $2p$ states. Molecular enhancements for the ($n=2$)-state population can be obtained from the ratios $P(2s)/P(2p)$ under assumption 1. Since the ratio $P(2s)/P(2p)$ for H_2^+ has not been given at present, assumption 1(c) is needed in this estimation. The results with H_2^+ for $n=2$ are plotted by open squares together with the regression curve best-fitted by Eq. (9) in Fig. 7. Brooks and Berry¹² also gave the model fit curve to the Lyman- α emission, $R_Y(2, t_D)$ versus t_D . Their curve can be converted to the relation $R_p(2, t_D) - 1$ versus t_D and the resultant curve is in excel-

lent agreement with our regression curve fitted by Eq. (9), at least in the $t_D (\leq 24 \text{ fs})$ region to which corresponding d value is 2 times greater than the average diameter of the $2s$ hydrogen orbit.

5. Projectile energy dependence of $R_p(n, t_D)$

To examine the energy dependence of $R_p(n, t_D)$, a regression analysis was made to the relation $R_p - 1$ versus t_D fitted by Eq. (9) for $n=3$ for H_2^+ with various energies. Most probable values of $R_p(3, 10 \text{ fs}) - 1$ were estimated by interpolation of values at 0.3, 0.4, 0.5, and 0.8 MeV/amu and are plotted by open circles in Fig. 8. Error bars indicate the 95% confidence intervals which correspond to twice standard deviations. The value $R_p(3, 10 \text{ fs}) - 1$ by Bukow *et al.*¹³ at 95 keV/amu was estimated by an interpolation to be 0.84 ± 0.19 (95% confidence interval) and is shown by a double circle in Fig. 8. For 50-keV/amu H_2^+ , the values $R_p(3, t_D) - 1$ were measured by Astner *et al.*¹⁵ for $t_D=6\text{--}13 \text{ fs}$. Their value at 10 fs was obtained by an interpolation and is shown by an open square in Fig. 8. For reference, $R_p(3, t_D) - 1$ measured by Andresen *et al.*¹⁴ are also shown by closed squares for 25-keV/amu ($t_D=55 \text{ fs}$) and 100-keV/amu ($t_D=27 \text{ fs}$) H_2^+ in Fig. 8. From Fig. 8, whether the value of $R_p(3, 10 \text{ fs}) - 1$ depends on the projectile energy or not is unclear at the present. However, if the data of Andresen *et al.* and Astner *et al.* for large t_D and low energies can be disregarded, we can see that the values $R_p(3, 10 \text{ fs}) - 1$ seem to be independent of projectile energy. Thus, in this work, the energy dependence is ignored for the energy range 0.3–0.8 MeV/amu. This is consistent with assumption 1(a).

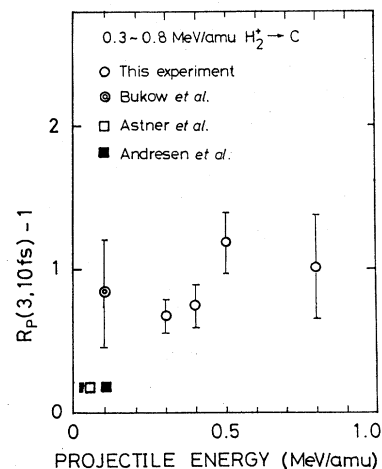


FIG. 8. Molecular enhancement $R_p(3, t_D) - 1$ as a function of projectile energy at $t_D=10 \text{ fs}$. Open circles are ours. A double circle is a value at $t_D=10 \text{ fs}$ interpolated from data of Bukow *et al.* (Ref. 9). Error bars indicate 95% confidence intervals. An open square is a value at $t_D=10 \text{ fs}$ derived from data of Astner *et al.* (Ref. 15). Solid squares are values at $t_D=27$ and 55 fs derived from data of Andresen *et al.* (Ref. 14).

6. n dependence of $R_P(n, t_D)$

One of the central problems in this paper is to determine the n dependence of the molecular enhancement, $R_P - 1$, at fixed dwell times and corresponding internuclear distances. In Fig. 9 are shown the values of $R_P(n, t_D) - 1$ as functions of n for $n = 2-5$ and $t_D = 2, 10$, and 20 fs. The values of $R_P - 1$ were obtained by interpolation of values given in Fig. 7 with error bars of the 95% confidence intervals and values for $n = 2$ shown by open circles were estimated from data of Brooks and Berry (see Sec. IV B 4). In Fig. 9, the molecular enhancement increases with increasing n at fixed t_D as predicted in Sec. IV B 3, and $R_P - 1$ seems to level off for $n \geq 3$ at ~ 2 fs which corresponds to the shortest dwell-time limit in the $t_D (\geq 2$ fs) region. This result may be interpreted as follows.

Let us consider the case with relatively larger t_D values. The dissociation mean free path of H_2^+ in the carbon foil can be estimated to be 24 Å at 0.8 MeV/amu from the transmission experiment² and is considerably smaller than the foil thicknesses in the present t_D region (≥ 100 Å). Thus, a major fraction of H_2^+ is dissociated at the depth corresponding to the mean free path and the internuclear distance d increases with increasing t_D by the Coulomb repulsion force. For instance, d increases from about 1.6 Å at 2 fs (corresponding to ~ 100 Å depth from the incident surface) to about 12 Å at 20 fs (~ 1000 Å), typically at 0.8 MeV/amu. In this d range, each of two protons

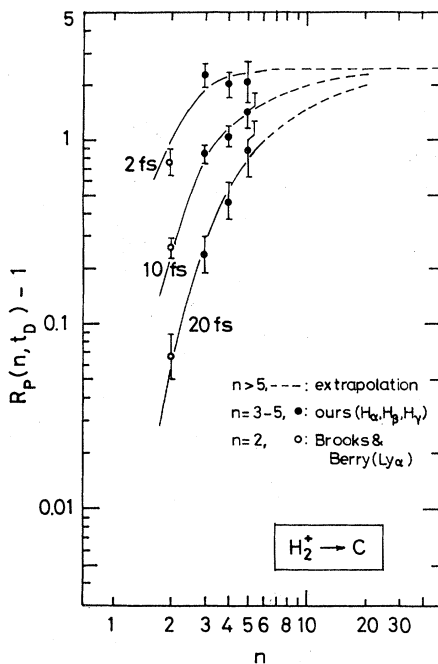


FIG. 9. Principal quantum number n dependence of molecular enhancements $R_P(n, t_D) - 1$ for (0.3–0.8)-MeV/amu H_2^+ at $t_D = 2, 10$, and 20 fs. Solid circles are our results. Open circles for $n = 2$ are derived from data of Brooks and Berry (Ref. 12). Error bars indicate 95% confidence intervals. Solid curves represent the best fitted curves to Eq. (9) and dashed curves are ones extrapolated from solid curves.

cannot capture an electron independently, since two wave functions corresponding to nl orbits of two hydrogen atoms should overlap on each other to form the linear combinations of atomic orbitals (LCAO). In other words, the probability of capture of an electron by one of two protons should be affected by the existence of another proton separated by the distance d . Thus, the capture process must occur on H_2^+ molecular orbital (MO) states with the distance d . Most of the formed H_2^+ MO states are regarded to be predissociating states of the molecular ion H_2^{+*} , which lead to $H(nl) + H^+$ breakup fragments.

The mean free path for electron loss of excited H_2^{+*} is not known at present. For H^0 , the mean free path for electron loss was measured to be ~ 18 Å at 0.8 MeV/amu by the transmission experiments.²⁶ Taking account of the fact that the dissociation mean free path for H_2^+ is 24 Å at 0.8 MeV/amu, the electron-loss mean free path for H_2^{+*} at 0.8 MeV/amu should be of the same order of magnitude as 24 Å or less. Then, the production of H_2^{+*} MO states which produce the observed dissociation fragment $H(nl)$ should mostly take place within the depth of about ten atomic layer from the exit surface and therefore the value d , at the moment for the electron capture to occur, can be approximated by that at the exit surface. From the above discussion, it is assumed that the electron capture into MO states near the exit surface may be the main process for productions of $H(nl) + H^+$ breakup fragments in the $t_D (\geq 2$ fs) region and consequently the electron-capture probability depends on d near the exit surface.

Cue *et al.*⁴ could successfully construct the reconstitution model for the observed transmitted yield of H_2^+ as well as the associated yield of $H(1s)$ breakup fragments. Their model is based on the assumption that the cross sections for electron capture into the MO (σ_c^g and σ_c^u), which correspond to the $1s\sigma_g$ and $2p\sigma_u$ states, can be expressed as

$$\sigma_c^{g,u} = [Z_{g,u}(d)]^5 \sigma_c^H, \quad (10)$$

where σ_c^H refers to the cross section for electron capture by a proton of the same velocity leading to an $H(1s)$ and $Z_{g,u}(d)$ characterizes the effective nuclear charge of the MO at d .

This model should be extended to other MO states which lead to more highly excited $H(nl)$ breakup fragments. The d -dependent effective charge for H_2^+ arises from a LCAO description as given by McCarroll *et al.*²⁷ Unfortunately, they calculated the $Z_{\text{eff}}(d)$ value only for the $H(1s) + H^+$ system, and $Z_{\text{eff}}(d)$ values for other MO states cannot be obtained at present. So we shall give hereinafter only qualitative discussions.

Let us consider the effective charge $Z_{\text{eff}}(r_c/d)$ as a function of the ratio r_c/d where r_c is a distance from the electron to be captured to the one of two protons (diproton). When r_c is much smaller than $d/2$ ($2r_c/d \ll 1$), $Z_{\text{eff}}(r_c/d)$ may approach unity and electron capture may occur to an individual proton. The effective charge $Z_{\text{eff}}(r_c/d)$ may increase with increasing r_c at a fixed d . If the screening effect due to the medium electrons could be neglected for swift projectiles as in the present case, the value of $Z_{\text{eff}}(r_c/d)$ would approach ~ 2 for $2r_c/d \gg 1$,

that is, the electron to be captured can see the two protons with distance d as if they form a united atom (diproton). Now, let us introduce a quantity $\langle r_c(n,d) \rangle$ which is defined as follows: $\langle r_c(n,d) \rangle$ is an average value of $r_c(n,d)$ averaged over the whole space and the whole MO states leading to breakup fragments $H(n)$. It is expected that higher-excited MO's which lead to a higher-excited fragment $H(n)$ are related to greater $\langle r_c(n,d) \rangle$ values, and thus to greater $Z_{\text{eff}}(\langle r_c(n,d) \rangle/d)$ values at a fixed d . The electron-capture cross section $\sigma_c^{\text{MO}}(n)$ to excited MO states corresponding to the production of $H(n)$ may be expressed as

$$\sigma_c^{\text{MO}}(n) = [Z_{\text{eff}}(\langle r_c(n,d) \rangle/d)]^s \sigma_c^{\text{H}}(n), \quad (11)$$

where $\sigma_c^{\text{H}}(n)$ is the cross section for electron capture into the excited hydrogen atom and s is a parameter and is generally not equal to the value ($s=5$) given in Eq. (10) for $1s\sigma_g$ and $2p\sigma_u$ MO states. The values of s were given for atomic ions on several theoretical models²⁸ but not for molecular ions. Using Eq. (11), the molecular effect for the population ratio of the n state in the t_D ($\gtrsim 2$ fs) region for H_2^+ is expressed as

$$R_p(n, t_D) = \frac{1}{2} \sigma_c^{\text{MO}}(n) / \sigma_c^{\text{H}}(n) \\ = \frac{1}{2} [Z_{\text{eff}}(\langle r_c(n,d) \rangle/d)]^s. \quad (12)$$

Consequently, it may be understood from the above discussion that the molecular enhancement for the production of $H(n)$ breakup fragments increases with increasing n at a fixed d [$=d(t_D)$] as shown in Fig. 9.

As seen from in Eq. (9), R_p approaches $k+1$ when t_D reduces to zero. It is found that k has an average value 2.50 ± 0.22 at $t_D=0$ which is obtained by extrapolation of $R_p(n, t_D) - 1$ curves for $n=3-5$ to $t_D=0$ in Fig. 7, where one has a relation $[2\langle r_c(n,d) \rangle/d] \gg 1$ for MO states leading to $n \geq 3$ excited breakup fragments. Then, in this small t_D region, $Z_{\text{eff}}(\langle r_c(n,d) \rangle/d)$ for $n \geq 3$ are close to 2. Therefore, R_p at $t_D=0$ is written from Eq. (12) as

$$R_p \sim 2^{s-1} \quad (13)$$

for $n=3-5$. This leads to $s=2.81 \pm 0.21$.

$R_p - 1$ values for the shortest t_D (~ 2 fs) in the t_D ($\gtrsim 2$ fs) region seem to level off for $n \geq 3$ in Fig. 9. As shown in the upper parts of Figs. 6 and 7, $t_D=2$ fs corresponds to $d=1.6$ Å which is much smaller than $\langle r_c(n,d) \rangle$ for the MO states, all of which lead to $H(n)$ ($n \geq 3$). Then, it may be concluded that in this small t_D region near 2 fs, $Z_{\text{eff}} \sim 2$, and R_p should be independent of n for $n \geq 3$.

V. SUMMARY

We measured the molecular effect for Balmer emission yields as functions of n and t_D for H_2^+ and H_3^+ incident on thin carbon foils for the beam energy range of 0.2–0.8 MeV/amu. The dependence of molecular effects for Balmer emission yields on $n=3-5$ was observed at $t_D=0.97-54.1$ fs. However, this n dependence diminishes with increasing t_D and finally disappears at $t_D \sim 54$

fs for 0.3-MeV/amu H_2^+ and H_3^+ and this result is consistent with data by Andresen *et al.*¹⁴ for larger t_D values (27 and 55 fs).

Next we estimated the n populations of $H(n)$ for H^+ , H_2^+ , and H_3^+ incident on carbon foils. The n -state population for incident H^+ follows the $n^{-2.30 \pm 0.11}$ scaling law (see Table II) for $n=3-6$ in the energy range 0.2–0.8 MeV/amu instead of the n^{-3} scaling law theoretically predicted²⁹ and the corresponding n -state populations for H_2^+ and H_3^+ also follow the n^{-2} scaling law similar to that for H^+ where z values decrease with increase of t_D as shown in Table II.

The molecular enhancement for the n -state populations of $H(n)$ from H_2^+ was derived for $n=3-5$. We also estimated the molecular enhancement for the ($n=2$)-state population using the experimental results of Brooks and Berry.¹² It was found that the molecular enhancement for the n -state population for H_2^+ decreases with increasing t_D and increases with increasing n , and is almost independent of the projectile energy in the energy range between 0.2 MeV/amu ($2.8v_0$) and 0.8 MeV/amu ($5.7v_0$) used in the present work. However, the molecular enhancement as a function of n seems to level off for $n \geq 3$ at the shortest dwell time ($t_D \sim 2$ fs) in the t_D ($\gtrsim 2$ fs) region.

The above result can be well interpreted in terms of the electron-capture probability related to the effective charge Z_{eff} of the diproton. The electron-capture cross section into the excited MO states of H_2^+ leading to the production of $H(n)$, $\sigma_c^{\text{MO}}(n)$, is derived from the experimental data as follows, for $t_D=0$:

$$\sigma_c^{\text{MO}}(n) = Z_{\text{eff}}^{2.81 \pm 0.12} \sigma_c^{\text{H}}(n), \quad n \geq 3, t_D = 0. \quad (14)$$

For the case in which the average distance from the nearest-neighbor proton to the electron to be captured is much larger than the internuclear distance of the diproton, $[2\langle r_c(n,d) \rangle/d] \gg 1$, Z_{eff} approaches 2. On the contrary, if $[2\langle r_c(n,d) \rangle/d] \ll 1$, Z_{eff} approaches 1. Equation (14) is contrasted with the expression given by Cue *et al.*⁴ with respect to the power of Z_{eff} ; $\sigma_c^{\text{MO}} = Z_{\text{eff}}^5 \sigma_c^{\text{H}}$. It should be noted here that the above interpretation is based on assumptions 1 and 2 stated in Sec. III, whose validity was discussed in some detail, but, in order to make the theoretical analysis more reliable, the experimental data on the relative substate population ratios for higher n (> 3) excited states for H^+ , H_2^+ , and H_3^+ , for t_D values longer than 20 fs are eagerly anticipated.

ACKNOWLEDGMENTS

The authors are grateful to T. Ichimori for several useful discussions and for giving us permission to quote some of his results prior to publication. The authors also extend their appreciation to F. Nishimura and Y. Yamazaki for helpful discussions and accelerator operation, and also to S. Ishizuka for construction of electrical circuits. We would like to thank T. Yonenaga, H. Naito, and A. Yasaka for the foil preparation and for their assistance in performing the experiments.

APPENDIX A: ESTIMATION OF CASCADE EFFECT

The cascading rearrangement effect can be estimated as follows. The populations of nl -substate levels at time t after exiting the foil, $P_{nl}(t)$, is determined from the following differential equation:

$$-\frac{dP_{nl}(t)}{dt} = \langle A_{nl} \rangle P_{nl}(t) + \sum_{n''=n+1}^{\infty} \sum_{l''=0}^{n''-1} [A_{n''l''nl} \delta(l'', l \pm 1)] P_{n''l''}(t), \quad (\text{A1})$$

where

$$\langle A_{nl} \rangle = \sum_{n'=1}^{n-1} \sum_{l'=0}^{n'-1} A_{nl'n'l'} \delta(l, l' \pm 1), \quad (\text{A2})$$

and $A_{nl'n'l'}$ is the transition probability from the nl to the $n'l'$ substate, δ is the delta function, and l , l' , and l'' are zero or positive integers. The exact solution of Eq. (A1) can immediately be written as

$$P_{nl}(t) = \exp(-\langle A_{nl} \rangle t) \left[P_{nl}(0) + \sum_{n''=n+1}^{\infty} \sum_{l''=0}^{n''-1} \left[A_{n''l''nl} \delta(l'', l \pm 1) \int_0^t P_{n''l''}(t) \exp(\langle A_{nl} \rangle t) dt \right] \right]. \quad (\text{A3})$$

Since the cascading rearrangement effect to the $n'' (> n)$ -state populations from more higher excited states ($> n''$) for the small t region gives only a negligibly small effect on the estimation of $P_{nl}(t)$ values, $P_{n''l''}(t)$ can be approximated as

$$P_{n''l''}(t) \simeq P_{n''l''}(0) \exp(-\langle A_{n''l''} \rangle t). \quad (\text{A4})$$

For instance, let us consider the $5g$ - $4f$ cascading rearrangement effect which should be the greatest contribution to the $n''=4$ state. The $5g$ state contributes only 0.3% to the $4f$ state at $t=8 \times 10^{-10}$ sec, which corresponds to the largest t value in our measurements. Therefore, the approximation given by Eq. (A4) is pertinent with respect to our experimental conditions. Equation (A3) becomes

$$P_{nl}(t) = \left[P_{nl}(0) - \sum_{n''=n+1}^{\infty} \sum_{l''=0}^{n''-1} \frac{A_{n''l''nl} \delta(l'', l \pm 1)}{\langle A_{nl} \rangle - \langle A_{n''l''} \rangle} \right] \exp(-\langle A_{nl} \rangle t) + \sum_{n''=n+1}^{\infty} \sum_{l''=0}^{n''-1} \frac{A_{n''l''nl} \delta(l'', l \pm 1)}{\langle A_{nl} \rangle - \langle A_{n''l''} \rangle} P_{n''l''}(0) \exp(-\langle A_{n''l''} \rangle t). \quad (\text{A5})$$

The emission intensity from the nl - $n'l'$ transition, $a_{nl'n'l'}$, at time t is expressed as

$$a_{nl'n'l'}(t) = A_{nl'n'l'} P_{nl}(t). \quad (\text{A6})$$

For the $3d$ - $2p$ transition, the intensity is approximated as

$$a_{3d2p}(t) \simeq A_{3d2p} P_{3d}(0) \exp(-A_{3d2p} t) - \frac{A_{3d2p} A_{4f3d}}{A_{3d2p} - A_{4f3d}} P_{4f}(0) [\exp(-A_{3d2p} t) - \exp(-A_{4f3d} t)], \quad (\text{A7})$$

where the transition from the $4p$ state and from $n'' > 4$ states can be ignored. Equation (A7) agrees with the corresponding formula given by Bukow *et al.*¹³

APPENDIX B: ESTIMATION OF $R_P(3, t_D)$ FROM DATA OF BUKOW *et al.*

From results of Bukow *et al.*,¹³ we can estimate $R_P(3, t_D)$ values in the following way. They have measured the initial $3d$ - $2p$ transition intensities a_{3d}^0 , as well as the initial population ratios $P(3d)/P(3s)$ and $P(3p)/P(3s)$, for H^+ , H_2^+ , and H_3^+ at various velocities. Molecular enhancement for the $n=3$ initial population can be estimated from their initial population ratios as follows:

$$R_P(3, t_D) \equiv \frac{P'(3d)}{P(3d)} \frac{P'(3s)/P'(3d) + P'(3p)/P'(3d) + 1}{P(3s)/P(3d) + P(3p)/P(3d) + 1}, \quad (\text{B1})$$

where $P(3d)$, $P(3p)$, and $P(3s)$ are initial substate populations for the proton, and $P'(3d)$, $P'(3p)$, and $P'(3s)$ for molecular ions. The values $P(3d)$ and $P'(3d)$ are related to the initial intensity a_{3d}^0 and the $4f$ - $3d$ cascade intensity a_{4f}^0 [Appendix A and Eq. (3) in Ref. 13]. From our estimation, a_{4f}^0 is found to be 6.2% and 7.0% of a_{3d}^0 for the proton and molecular ions, respectively. Therefore, $P'(3d)/P(3d)$ is approximated by neglecting the cascade intensity within 0.8% errors as

$$\frac{P'(3d)}{P(3d)} \simeq \frac{(a_{3d}^0)' + (a_{4f}^0)'}{a_{3d}^0 + a_{4f}^0} \simeq \frac{(a_{3d}^0)'}{a_{3d}^0}, \quad (\text{B2})$$

where $(a_{3d}^0)'$ and $(a_{4f}^0)'$ denote initial intensities for the molecular ions.

- *Permanent address: Institute for Atomic Energy, Rikkyo University, 2-5-1 Nagasaka, Yokosuka, Kanagawa 240-01, Japan.
- ¹M. J. Gaillard, J. C. Poizat, A. Ratkowski, J. Remillieux, and M. Auzas, *Phys. Rev. A* **16**, 2323 (1977).
- ²J. Remillieux, *Nucl. Instrum. Methods* **170**, 31 (1980).
- ³M. J. Gaillard, J.-C. Poizat, A. Ratkowski, and J. Remillieux, *Nucl. Instrum. Methods* **132**, 69 (1976).
- ⁴N. Cue, N. V. de Castro-Faria, M. J. Gaillard, J.-C. Poizat, and J. Remillieux, *Phys. Rev. Lett.* **45**, 613 (1980).
- ⁵N. Cue, M. J. Gaillard, J. C. Poizat, J. Remillieux, and J. L. Subtil, *Phys. Rev. Lett.* **42**, 959 (1979).
- ⁶N. Cue, N. V. de Castro-Faria, M. J. Gaillard, J. C. Poizat, and J. Remillieux, *Phys. Lett.* **72A**, 104 (1979).
- ⁷R. Laubert and F. K. Chen, *Phys. Rev. Lett.* **40**, 174 (1978).
- ⁸M. J. Gaillard, J. C. Poizat, and J. Remillieux, *Phys. Rev. Lett.* **41**, 159 (1978).
- ⁹E. P. Kanter, P. J. Cooney, D. S. Gemmell, K.-O. Groeneveld, W. J. Pietsch, A. J. Ratkowski, Z. Vager, and B. J. Zabransky, *Phys. Rev. A* **20**, 834 (1979).
- ¹⁰D. S. Gemmell, *Proceedings of the 6th International Congress on Radiation Research, Tokyo*, edited by S. Okada, M. Imamura, T. Terashima, and H. Yamaguchi (University of Tokyo, Tokyo, 1979), p. 132.
- ¹¹G. Gabrielse, *Phys. Rev. A* **23**, 775 (1981).
- ¹²R. L. Brooks and H. G. Berry, *Phys. Rev. A* **25**, 161 (1982).
- ¹³H. H. Bukow, H. v. Buttler, D. Haas, P. H. Heckmann, M. Holl, W. Schlagheck, D. Schürmann, R. Tielert, and R. Woodruff, *Nucl. Instrum. Methods* **110**, 89 (1973); R. Tielert, H. H. Bukow, P. H. Heckmann, R. Woodruff, and H. v. Buttler, *Z. Phys.* **264**, 129 (1973).
- ¹⁴B. Andresen, S. Hultberg, B. Jelenković, L. Liljeby, S. Mannervik, and E. Veje, *Phys. Scr.* **19**, 335 (1979); *J. Phys. (Paris) Colloq.* **40**, C1-352 (1979).
- ¹⁵G. Astner, S. Mannervik, and E. Veje, *Phys. Rev. A* **25**, 828 (1982); *Nucl. Instrum. Methods* **194**, 319 (1982).
- ¹⁶H. Kobayashi and N. Oda, *The XIIIth International Conference on the Physics of Electronic and Atomic Collisions, Gatlinburg, Tennessee, 1981*, edited by S. Datz (North-Holland, Amsterdam, 1981), Vol. 2, p. 994; *J. Phys. Soc. Jpn.* **51**, 2715 (1982).
- ¹⁷H. Kobayashi and N. Oda, Oak Ridge National Laboratory Report No. 820131, 1982 (unpublished); *Nucl. Instrum. Methods* (to be published).
- ¹⁸H. H. Andersen and J. F. Ziegler, *Hydrogen Stopping Powers and Ranges in All Elements*, Vol. 3 of *The Stopping and Ranges of Ions in Matter* (Pergamon, New York, 1977).
- ¹⁹W. L. Wiese, M. W. Smith, and B. M. Glennon, *Hydrogen Through Neon*, Vol. 1 of *Atomic Transition Probabilities*, Natl. Bur. Stand. (U. S.), Nat'l. Stand. Ref. Data Ser. No. 4 (U. S. GPO, Washington, D. C., 1966).
- ²⁰M. J. Alguard and C. W. Drake, *Phys. Rev. A* **8**, 27 (1973).
- ²¹W. S. Bickel, *J. Opt. Soc. A* **58**, 213 (1968).
- ²²F. Hopkins and P. v. Brentano, *J. Phys. B* **9**, 775 (1976).
- ²³For example, E. Kreyszig, *Introductory Mathematical Statistics, Principle and Methods* (Wiley, New York, 1970).
- ²⁴M. J. Gaillard, D. S. Gemmell, G. Goldring, I. Levine, W. J. Pietsch, J. C. Poizat, A. J. Ratkowski, J. Remillieux, Z. Vager, and B. J. Zabransky, *Phys. Rev. A* **17**, 1797 (1978).
- ²⁵H. A. Bethe and E. E. Salpeter, *Quantum Mechanics of One- and Two-Electron Atoms* (Springer, Berlin, 1957).
- ²⁶N. Cue, N. V. De Castro Faria, M. J. Gaillard, J. C. Poizat, and J. Remillieux, *Nucl. Instrum. Methods* **170**, 67 (1980).
- ²⁷R. McCarroll, R. D. Piacentini, and A. Salin, *J. Phys. B* **3**, 137 (1970).
- ²⁸R. Shakeshaft, *Rev. Mod. Phys.* **51**, 369 (1979).
- ²⁹M. C. Cross, *Phys. Rev. B* **15**, 602 (1977).